PCCP

15

ARTICLE TYPE

Cite this: DOI: 00.0000/xxxxxxxxxx

Effect of the sulfur termination on the properties of Hf_2CO_2 MXene

Chewki Ougherb,*[a] Tarik Ouahrani*[a], Michael Badawi[b], and Ángel Morales-García*[c]

Received Date
Accepted Date

DOI: 00.0000/xxxxxxxxxx

First-principles calculations are performed to investigate the effect of surface termination of MXenes. In particular, we focus on the Hf_2CO_2 and Janus Hf_2COS MXene. The present study confirms that the breaking of the structural symmetry generated by the chemical substitution of the O surface layer by S ones, promotes the tuning of the electronic properties. Hf_2CO_2 behaves as a semiconductor and its band gap is reduced, increasing the concentration of S atoms. Indeed, Hf_2COS is metallic. In short, the present study confirms that tailoring the surface termination of MXene emerges as a suitable strategy to change the properties of MXene. Additionally, such a change in surface termination affects both vibrational frequencies and the rigidity of the Hf_2CO_2 MXene.

1 Introduction

Low dimensional carbides and nitrides, known as MXenes, have generated great expectations since their synthesis a bit over a decade ago [1–3]. MXenes have shown extraordinary electronic, optical, and mechanical properties, leading to applications covering energy storage [4], catalysis [5,6], biomedical [7], and electronic applications, to name a few [8,9]. Not surprisingly, this broad landscape of applications is directly connected with the atomic composition of MXenes. These bidimensional materials are described with the chemical formula ($M_{n+1}X_n$ T_x, where n=1, 2, or 3) where M, X, and T_x stand for an early transition metal, carbon, or nitrogen, and the termination or functionalization of MXene (i.e., -O, -F, and -OH mainly). The synthesis of MXenes follows a top-down procedure where the parental MAX precursor is selectively etched, removing the A (i.e., **p**-block element) that connects the MXene layers. Depending on the chemical agents [10,11] used during the etching, the functionalization of MXenes is different. Indeed, the properties of MXene materials could be modified by modulating their surface chemistry. These terminating groups were shown a random distribution over the surface with limited experimental control over their composition [2]. Fortunately, computational simulations [12] have shown that these surfaces can also be covered by uniform terminations of T_x.

Recently, MXenes have emerged as candidates as sulfur (S) hosts, making them suitable for sulfur battery applications [13,14]. Topologically speaking, the new surfaces possess bonded intermediate polysulfides via metal-sulfur interaction, which enhances their conductivity. For instance, S/Ti_2C constitutes a material with a stable long-term cycling performance with a high specific capacity, due to the strong interaction of the polysulfide species with the surface M atoms. Experimental investigations have established that the habitual OH termination of this monolayer could be replaced by S atoms at high temperatures, promoting new functionality for the resulting MXene-derived material [15]. However, the former terminations (i.e., O, OH, and F) dominate the surface chemistry, and aside from Nb and Ta MXene carbides [16], the literature of S-terminated MXenes is limited.

Revising the literature, one finds that O-functionalized MXenes like Ti_2CO_2, Zr_2CO_2, and Hf_2CO_2 attained growing attention, due to their moderate bandgap and high carrier mobility in comparison to other MXenes [17]. Among them, Hf-based MXenes have been reported to be stable whether the termination surfaces are fully replaced by the sulfur atoms [18]. Indeed, the calculation of S or O adsorption on the bare Hf_2C monolayer was found favorable on its hollow site, allowing the construction of Hf_2CO_2 or Hf_2CS_2 MXenes. Furthermore, different functionalities have been explored by considering the use of two different terminations of the MXene, constituting Janus structures [19]. The atomic structure of these particular MXenes breaks the out-of-plane symmetry by different terminations (see Figure 1). Indeed, Ti_2CST_x (T_x= O, Se) for example, was recently investigated for its valuable electrochemical properties and reasonable diffusion barriers as a Li and Mg electrode application [20]. This study reported that Ti_2CST_x Janus-like Mxene structure is thermodynamically stable exhibiting a high gravimetric capacity, which makes it a candidate to alternate conventional Li sources for rechargeable battery

[a]*Laboratoire de Physique Théorique, Université de Tlemcen 1300 Algeria; E-mails: chewki2002@yahoo.fr, tarik_ouahrani@yahoo.fr*
[b] *Université de Lorraine and CNRS, LPCT, UMR 7019, 54506 Vandoeuvre-lés-Nancy, France*
[c]*Departament de Ciència de Materials i Química Física & Institut de Química Teòrica i Computacional (IQTCUB) Universitat de Barcelona, Spain; E-mail: angel.morales@ub.edu*

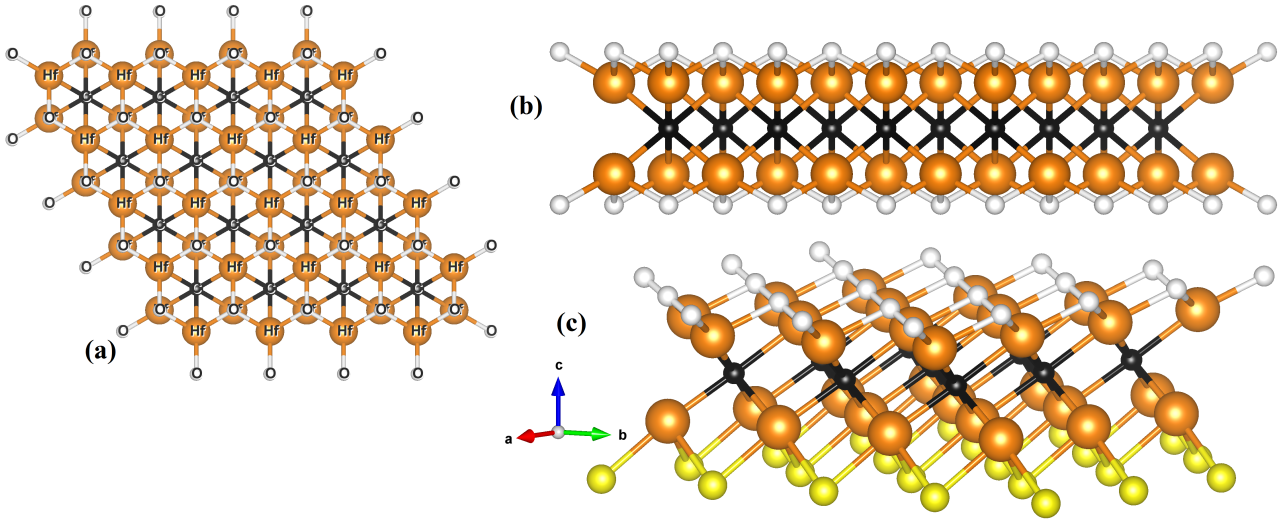

Fig. 1 (a) the top and (b) the side views of Hf_2CO_2 Mxene monolayer. The (c) plot gives its Janus structure. Orange, white, black, and yellow spheres represents Hf, O, C and S atoms, respectively.

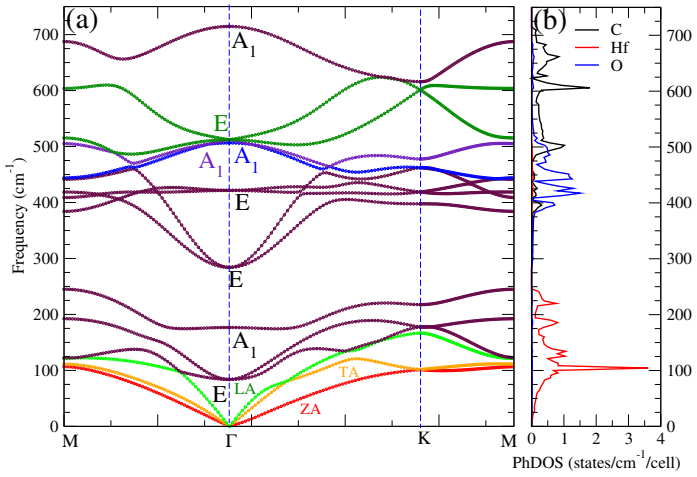

Fig. 2 Phonon dispersion and phonon density of states (DOS) curves of Hf_2CO_2 MXene monolayer at zero pressure. The partial DOS (PDOS) projected onto C, Hf and O are also presented with black, red, and blue, respectively. The out-of-plane acoustic (ZA), longitudinal acoustic (LA) and transversal acoustic (TA) modes are colored with red, orange, and green, respectively.

devices.

Actually, the spotlight is focused on low-dimensional materials composed of Hf atoms in their atomic structure. Some studies have suggested several candidate materials such as heterostructures, or monolayer systems[21–23]. For instance, the highly stable $Hf_2CO_2$is a semiconducting material with an energy gap of ~ 1.70 eV. Narrowing its energy gap makes it suitable for infrared or thermoelectric applications, whereas opening the gap makes power electronics and optoelectronic functionality accessible. One way to modulate the electronic properties is to use chemical strategies by inducing the substitution of O-terminated atoms. Indeed, this is the goal of the present study: tune the electronic properties of Hf_2CO_2 MXene by replacing the O-termination atom with

Table 1 Calculated optical frequencies (ω) (in cm^{-1}) of Hf_2CO_2 and Hf_2COS MXene structures

	Hf_2CO_2	Hf_2COS
mode	ω(cm^{-1})	ω(cm^{-1})
A1	176.7	166.2
A1	506.4	341.8
A1	511.9	489.7
A1	714.6	659.1
E	284.1	178.1
E	421.6	314.6
E	512.2	478.9
E	83.9	85.0

the S-terminations. These termination exchanges will allow us to modulate the electronic and optical properties of this MXene. In addition, we will evaluate the stability of the MXene Janus by analyzing its thermodynamical, mechanical, and dynamical properties.

2 Computational strategy

In the present study, first-principles calculations are performed by using the projector augmented plane wave potential (PAW)[24] implemented in the Vienna Ab initio Simulation Package (VASP)[25,26]. For the exchange-correlation functional, we employed the generalized gradient approximation (GGA), proposed by Perdew, Burke, and Ernzerhof (PBE)[27]. The self-consistent calculations were judged to have converged to a tolerance of less than 10^{-8} eV, and the Hellman-Feynman force on each relaxed atom was less than 0.006 eV/Å. Due to the presence of oxygen in the investigated material, the set of plane waves was extended up to a kinetic energy cutoff of 700 eV. The integrations over the Brillouin zone (BZ) were calculated with a dense gamma grid of special k points with a mesh of $7\times7\times1$. To overcome the limitations of traditional density functionals to reproduce band gap value[28], we used the Heyd-Scuseria-Ernzerhof (HSE) hybrid density functional (HSE06)[29] calculated over a single point calculation of the

PBE structure. Furthermore, lattice-dynamics calculations were performed by the means of PHONOPY[30] open-source package interfaced to VASP code. This code uses the density-functional perturbation theory (DFPT)[31] to estimate the force constant within the supercell method. Thus, a large supercell $p(2\times2)$ of Hf_2CO_2 MXene containing 20 atoms (4 C, 8 Hf, and 8 O atoms) was modeled within a 20 Å vacuum along the z-axis to avoid interactions between the adjacent molecules and slabs, respectively. Noting that a similar supercell was used for the Hf2COS. Here, the dispersion correction was assured by the use of the DFT-D3 approach of Becke-Jonson damping[32,33]. Finally, the thermal stability was checked by carrying out molecular dynamics (MD) based-simulations. The MD was performed within the NVT ensemble and controlled by the Nose-Hoover method[34–36], with a time step of 1fs within the microcanonical ensemble, i.e., the total energy was conserved during the simulations. This energy conservation was typically fulfilled to within ±5 meV along an AIMD run.

3 Results and Discussion

3.1 Stability of pristine Hf_2CO_2 MXene structure

Hf_2CO_2 is a layered material composed of five atomic layers, in which the carbon layer is sandwiched between two hafnium layers, and these are functionalized by oxygen atoms. In this study, we consider only its more stable octahedral T1 structure a ABCAB stacking[37], and a space group P3m1 (No. 156), with a point group of C_{3v} (Figures 1(a) and 1(b)). The optimized thickness (t) and lattice constant (a) were found to be equal to 4.59 and 3.27Å, being the latter in excellent agreement with the value reported in the literature[38,39]. The first analysis is the thermodynamic, and mechanical stability. Thus, calculations of phonon dispersion, elastic constant, and molecular dynamic simulation are carried out. Figure 2 depicts the phonon dispersion of the pristine Hf_2CO_2 material along the armchair (Γ–M) and zigzag (Γ—K) directions. The phonon spectrum of Hf_2CO_2 in its 1T-type phase is free of imaginary frequencies in the first Brillouin zone, indicating the thermodynamic stability of Hf_2CO_2 MXene, consistent with a previous study[37]. It is observed that the longitudinal acoustic (LA) and transverse acoustic (TA) branches of MXene Hf_2CO_2 are linear when the wave vector q is close to the center of the Brillouin zone. However, the acoustic (ZA) branch in the **z**-direction deviates from this trend owing to the sufficiently weak interplanar interactions, which is in concordance with the microscopic elastic theory, which is a generic feature of the monolayer material[40]. The analysis of the zone center phonons gives the following mechanical decomposition : Γ_{optic} = $4A_1$ + 4E, whereas, $\Gamma_{acoustic}$ = A_1 + 2E, resulting in 12 optical modes and three acoustic modes at the center of the Brillouin zone, Γ. It is also noticed that in the phonon spectra, the modes for $\omega(E)$= 421.6 and 506.4 cm^{-1} are both doubly degenerated. The calculated modes are gathered in Table 1.

Furthermore, it is important to understand the mechanical properties of the Hf_2CO_2 MXene structure by analyzing the elastic stiffnesses ($\mathbb{C}_{ij}$) matrix. Due to symmetry reasons, we have only two elastic stiffness components, C_{11} and C_{12}, the C_{66}= (C_{11} - C_{12})/2. Given the bidimensional nature of the MXene structures, the in-plane mechanical properties. This analysis is summarized in Table 2, where one can see clearly that Hf_2CO_2 MXene meets the Born criteria of mechanical stability ($C_{11} > 0$ and $C_{66} > 0$). Further dynamical descriptors such as Young modulus (E), Area modulus (K), Shear modulus (G), and Poisson ratio (ν), which are required to evaluate the material's response to applied pressure, were evaluated. The K, G, and E results, as summarized in Table 2, show that the Hf_2CO_2 MXene structure is rather rigid and non-compressible, even if the response to shear direction is weak. Therefore, applying constraint force on the transverse section during uniaxial tension or compression will weakly affect the compound. Furthermore, the value of the in-plane Poisson's ratio (ν) indicates that the structural stability of the Hf_2CO_2 MXene is assured due to its greater thickness, higher than other bidimensional monolayers, like the MoS_2[41,42], the C_{11}, is too large in comparison to the C_{12}. This indicates that axial compression requires larger forces than shear and tensile deformations. From the elastic constants the area (K), Young (E), and shear (G) moduli can be obtained. We have found that $E > K > G$ is in agreement with our previous conclusion. This MXene also shows a clear isotropic feature along with the a and b directions. This statement is compatible with the isotropic trend of the structure found close to 1. Furthermore, the thermal stability of Hf_2CO_2 was also qualitatively tested at 300 K and 700 K by AIMD simulation with the mole–volume–temperature (NVT) ensemble[34–36]. The total energy oscillation and temperature displayed in Figure 3 indicate no bond-breaking or structural distortion of the Hf_2CO_2 MXene structure after 5 ps. This accurate analysis of the stability indicates the noted stability of Hf_2CO_2 MXene at room temperature and even at high temperatures.

Table 2 Calculated elastic constants C_{ij} (GPa) of $MgPSe_3$ monolayer. The table gives also the Young modulus (E (GPa)), Area modulus (K (GPa)), Shear modulus (G (GPa)), Poisson ratio (ν).

	C_{11}	C_{12}	C_{66}	E	G	K	ν
Hf_2CO_2	241.41	75.59	82.91	217.74	82.91	158.51	0.31
Hf_2COS	186.41	50.22	68.09	172.88	68.09	118.31	0.27

3.2 Structural, dynamical and mechanical properties of Hf_2COS MXene structure

Let us now deal with the substituted Hf_2CO_2 MXene structure. Our strategy is to study the properties of the Janus structure (Hf_2COS) first, and later analyze the effect of sulfur substitution on the surface of the Hf_2COS. By this, we will use the effect symmetry break to modulate the properties of Hf_2COS. The Janus structure is shown in Figure 1(c). We start analyzing the dynamical stability of the Janus by performing phonon calculations. The corresponding plot is displayed in Figure 4 along with the phonon density of states. The dispersion plot is shown to be free of soft modes, indicating Janus's dynamic stability. Some differences are noticed in comparison to the plot of the MXene Hf_2CO_2 (Figure

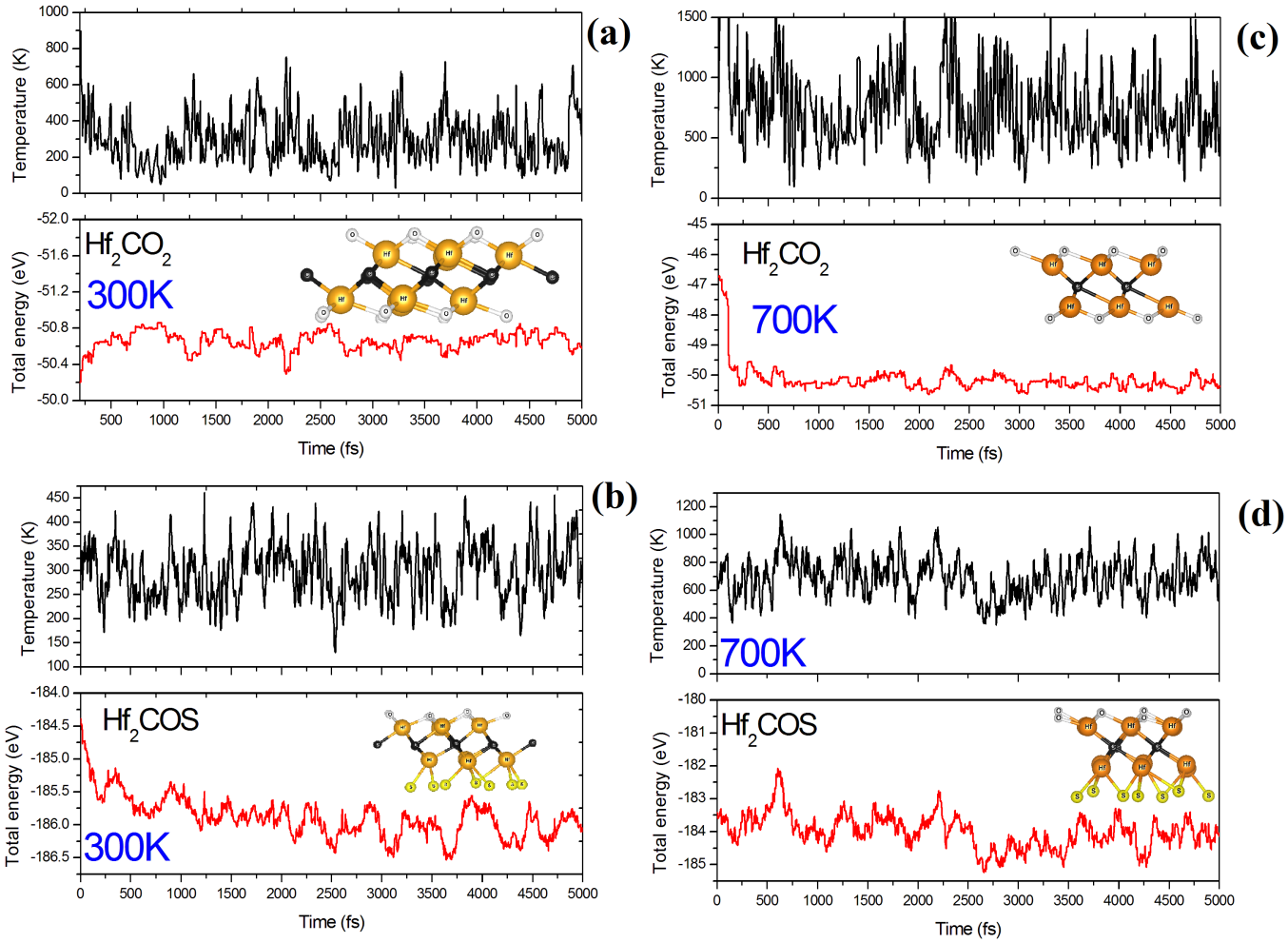

Fig. 3 MD simulation of temperature oscillations and energy fluctuations as a function of MD simulation time step at T= 300 and 700 K (a),(c) for Hf_2CO_2 and (b),(d) for Hf_2COS structures

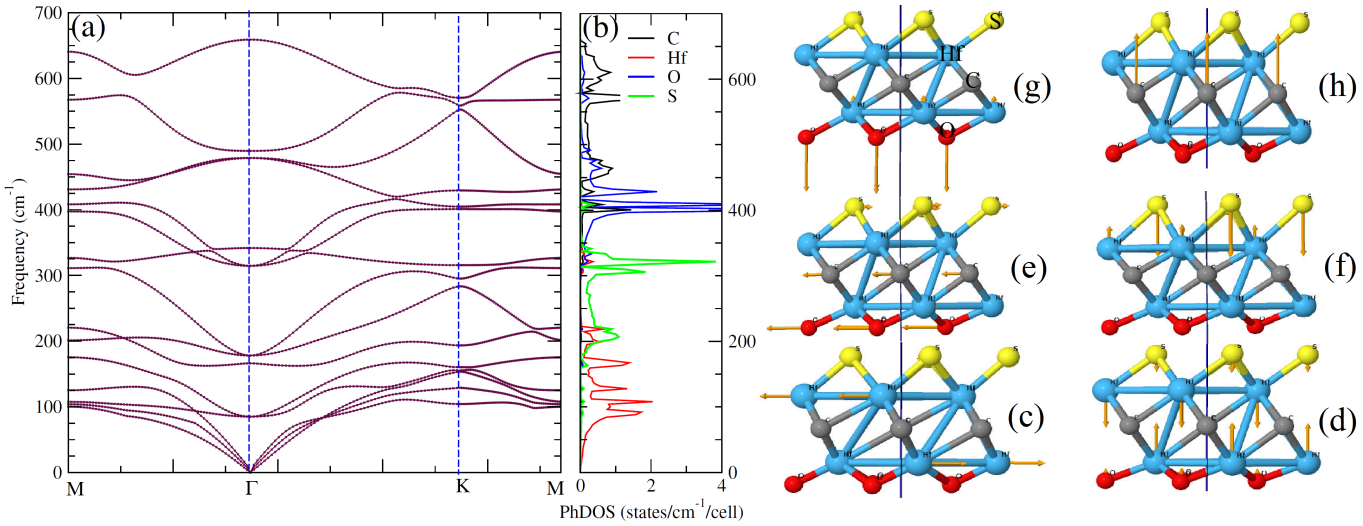

Fig. 4 Phonon dispersion and phonon density of states curves of Hf_2COS Mxene Janus at zero pressure. The partial DoS (PDoS) projected onto C, Hf, O and S are also presented with black, red, blue, and green respectively. The phonon eigenvectors of some modes are also shown, (c) 85.0 cm^{-1}, (d) 166.2 cm^{-1}, (e) 314.6 cm^{-1}, (f) 341.8 cm^{-1}, (g) 489.7 cm^{-1} and (h) 659.1 cm^{-1}.

2) ; namely, the ZA mode nearly coincides with the TA mode in the armchair direction, differing from that along the zigzag direction. Furthermore, the mode attributed to the sulfur atoms fills the emptiness shown in Figure 2 between the Hf and oxygen ones in the Hf_2CO_2 MXene. We can identify the corresponding mode for each atom by plotting its phonon eigenvector representation, see Figures 4(c)– 4(f). The vibration of atoms in the low frequencies originates from the Hf atoms. This movement should be weak due to the strong covalent Hf–C bonds. Also, the modes at high frequencies are rather derived from the carbon of oxygen atoms, and they do not appear to induce any distortion in the polyhedra. However, the modes between 250 cm^{-1} and 350 cm^{-1} originate from the sulfur vibrations in a number of directions. They are related to stretching vibrations, which result in the shearing of the S atoms around the Hf one, which could be responsible for increasing the effect of the symmetry break. Indeed, there are two frequencies with wavenumbers, 314.6 cm^{-1} and 341.8 cm^{-1} that are "isolated" from the rest of the modes. These correspond to normal motions of atoms inside the octahedra forming the functionalized surfaces, while the other external modes involve motions of rigid units against the C and Hf atoms.

Another interesting result is the lifting of the degeneracy of some modes shown in the phonon dispersion plot of the Janus structure. The new packed phonon branches could decrease the rigidity of the material. To deeply investigate this behavior, we also calculated elastic properties and the corresponding Young and Shear modulus. The results are gathered in Table 2 together with those of Hf_2CO_2 MXene. It seems that in the Janus structure, both the Young and Shear values decrease by 20% and 18%, respectively. The Poisson ratio is also affected; its value changed from 0.31 to 0.27. This means that the breaking of symmetry affects not only the vibrational modes of the structure but also its chemical nature. The AIMD simulation of the Janus Hf_2COS structure reveals a periodic trend in both temperature and total energy at ambient temperature, demonstrating that the structure is thermodynamically stable (see Figure 3).

3.3 Analysis of the electronic and bonding properties

Substituting the oxygen atoms with the sulfur ones in the Mxene compounds is a good choice in principle because S and O are the nearest congeners in the Periodic Table. However, due to the difference in electronegativity χ(O)=3.5 and χ(S)=2.5, we expect some differences in electronic and bonding properties between Hf_2CO_2 MXene and its partially S-terminated structures. According to published work, fully sulfurized Hf_2CS_2 [18] exhibits metallic behavior, whereas pristine Hf_2CO_2 has a theoretical band gap of 1.79 eV[43] and varies between 1.66 eV[44] and 1.59 eV[45] with the HSE06 approximation. We have performed hybrid HSE06 calculations in order to analyze the band gap value change between Hf_2CO_2 MXene and Janus states. The obtained results are gathered in Figure 5. The figures show band structures and partial densities of states. The calculated band gap of Hf_2CO_2 MXene is indirect, with a value of 1.64 eV, which is in excellent agreement with the available results. One observes that the C-2*p* is the more dominating orbital near the Fermi level of the pristine material,

Table 3 QTAIM analysis of Hf_2CO_2 and Hf_2COS structures

	Hf_2CO_2		Hf_2COS	
atom	$\mathcal{Q}$	T	$\mathcal{Q}$	T
C	-2.07	51.64	-0.96	23.95
Hf	2.39	59.96	1.86	46.58
O	-1.35	67.65	-1.29	64.64
S	–	–	-0.52	64.64

and the conduction band is attributed to Hf-*d* orbitals, while the substitution of one T_x surface makes the S-2*p* the major contribution of the energetic level in the more high band valence states. We can state that in the case of semiconducting Hf_2CO_2 MXenetion shifts the Fermi energy to the center of the gap between the Hf *d* bands and the C *p* bands. However, when we make a non-symmetric surface termination, the Fermi energy becomes located at the *d* bands of transition Hf metal. The valence band maximum states are located at the Γ point and are primarily composed of C-$_{p_x+p_y}$ orbitals hybridized with O-$_{p_x+p_y}$ and Hf-$_{d_{xz}+d_{yz}}$. We remark that the substitution of an oxygen atom with a sulfur one makes the level of C-2*p* slightly flatten and shift downwards from the Fermi level. This makes the electron come from sulfur atom-like impurities intentionally added to a host semiconductor. The substitution builds an acceptor state above the valence band from the S-2p level, which elevates the maximum of the valence band and favors the photo-generated holes to maintain high mobility[46].

To emphasize the difference between the studied structures, we performed additional calculations on bonding properties. We do so by performing bander charge analysis[47,48] and using the reduced gradient of the electron density (s)[49,50] to reveal the nature of interactions governing each monolayer, see Figure 6. Hence, effective charges $\mathcal{Q}$, charge transfer T were calculated and summarized in Table 3. By simply adding the ratios of these effective charges ($\mathcal{Q}(\Omega)$) with respect to the corresponding nominal oxidation states ($OS(\Omega)$) for the N atoms of the formula unit, we evaluate an index that measures the degree of ionicity of this structure[51]: $\alpha = \frac{1}{N}\sum_{\Omega=1}^{N}\frac{\mathcal{Q}(\Omega)}{OS(\Omega)}$. While the Hf_2CO_2 MXene has a more ionic nature (α= 61.37%), the Janus structure has a more covalent nature (α= 49.28%). As a result, replacing one surface termination T_x of the Hf_2CO_2 MXene with sulfur atoms causes not only metalization but also an increase in the number of interactions due to the change in bonding length[52]. Such interactions, for example, can be observed in the s isosurface depicted in Figure 6. For the sake of comparison, the plots for pristine and Janus structures are displayed together. The fact that the green electronic domain dominates the cell, is clear proof of strong van der Waals interactions. Furthermore, we can clearly show that blue/red spike isosurfaces govern the Hf–O bonds, whereas the interactions around the Hf–S bonds are purely repulsive. The red domains correspond to covalent bonding, while the blue domains correspond to ionic bonding, implying that both structures have a mixed bonding, but the covalency is stronger in the Janus structure.

Although the sulfurization of MXene's surface was done by experience with nonuniform methods[53], theoretical studies[54–56] demonstrate that the substitution of groups of surface can also

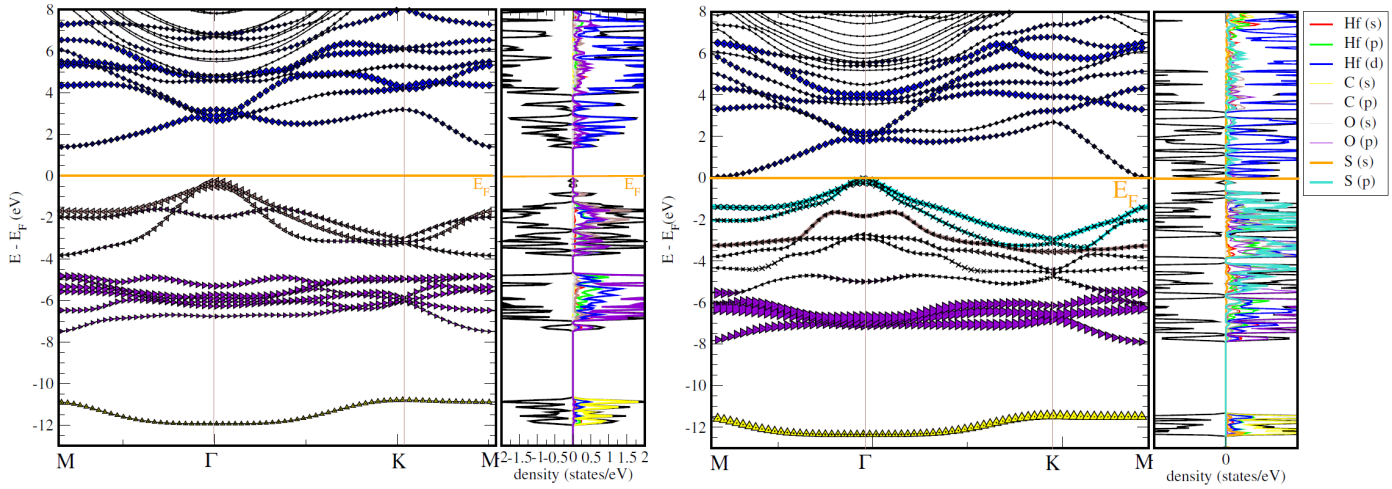

Fig. 5 HSE06 band structures and partial densities of states, left for Hf_2CO_2 and right for Hf_2COS structures

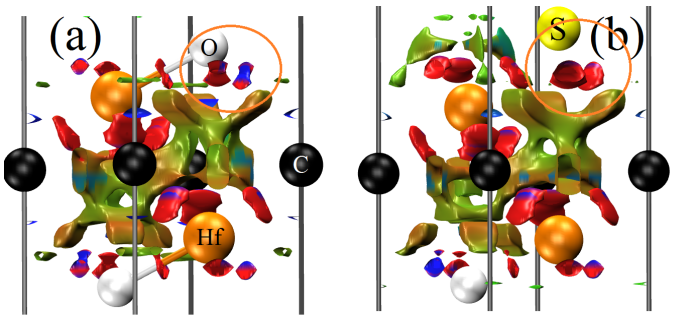

Fig. 6 views of NCI isosurfaces of Hf_2CO_2 and Hf_2COS structures

be done in a uniform way, giving rise to more stable structures. Indeed, sulfur substitutions were uncommon; some preliminary work was done using solvent effects with a focus on interlayer intercalation[57]. In this regard, and because the effect of T_x termination can act as a standpoint to shift the value of the band gap, we use three structural configurations to tune the electronic properties of the investigated compound: $Hf_2CO_{7/8}S_{1/8}$, $Hf_2CO_{6/8}S_{2/8}$ and $Hf_2CO_{5/8}S_{3/8}$. However, the symmetric substitution of O atoms with S was also tested in order to check the effect of breaking symmetry. In Figure 7(a), we summarize the calculated band gap values for the three tested configurations. We found that the band gap is strongly affected by the concentration of sulfur atoms. We also notice that the substitution with a sulfur atom changes the nature of the band gap to one that is direct (see Figure 7(b), allowing a direct transition from the valence to the conduction band. Thus, owing to the change in band gap values, we can stipulate that passivation of Hf_2C by functional groups like sulfur atoms can activate this material for many applications[58], ranging from storage applications to photovoltaic applications[59].

4 Conclusions

In this paper, we demonstrate how the surface termination can be used for tailoring the electronic properties of the Hf_2CO_2 MXene material by using DFT-based calculations. We focus on the study of the Hf_2CO_2 and Janus Hf_2COS MXene. Our analysis was done by performing phonon dispersion and calculating the elastic components. We have shown that the vibrational frequencies are affected by the sulfurization, even though the symmetry is not changed. The breaking of symmetry by the T_x surfaces causes a decrease in rigidity. In addition, the band gap values are different according to the surface group termination.

Indeed, the partial density of states shows that the T_x group can tune the position of Hf-*d* and the C-*p* states, resulting in either semiconducting or metallic states. According to the Bader charge calculation, changing the oxygen groups by sulfur ones increases the covalency of the material, and this change is attributed to an increase in repulsive interaction around the Hf–O, and Hf–S bonds. Finally, our calculations show that the uniform substitution of an oxygen atom with a sulfur atom can be a useful tool for tuning the band gap value of the investigated material, allowing the Hf_2CO_2 Mxene to be used in a variety of device applications.

Data availability

All relevant data are available from the corresponding author upon reasonable request.

Declaration of competing interest

The authors declare that they have no known competing financial interests or personal relationships that could have appeared to influence the work reported in this paper.

Acknowledgements

C.O. acknowledges the financial support given by the Laboratory of Theoretical Physics of the University of Tlemcen. A. M.-G. thanks the support by the Spanish MICIN through the project PID2020-115293RJ-I00/AEI/10.13039/501100011033 and

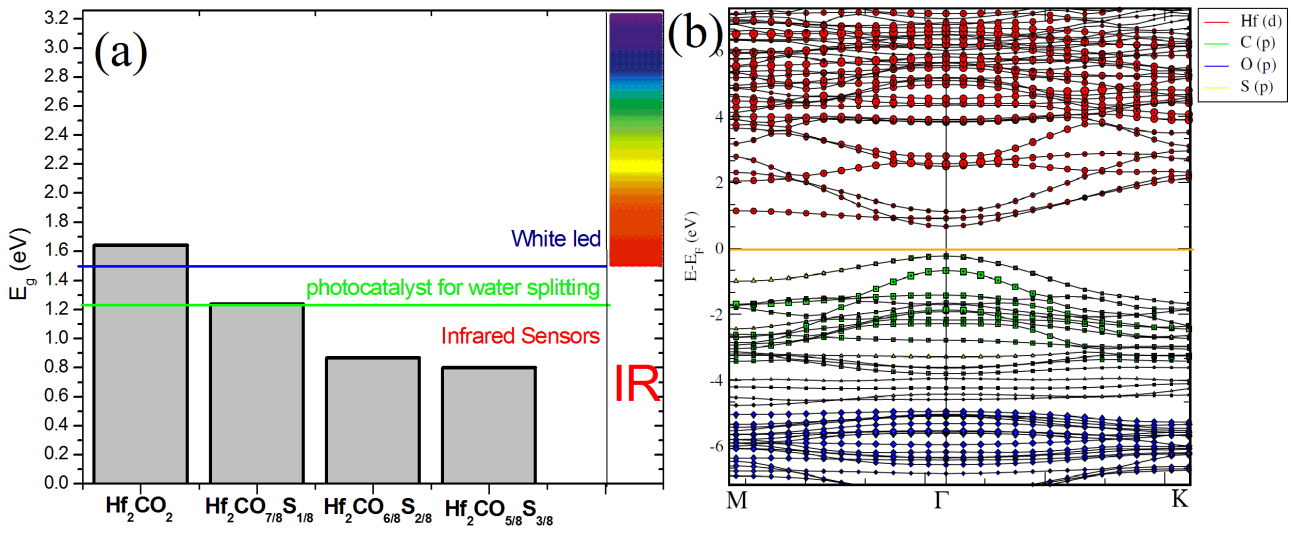

Fig. 7 (a): diagram of band gap values of $Hf_2CO_{7/8}S_{1/8}$, $Hf_2CO_{6/8}S_{2/8}$ and $Hf_2CO_{5/8}S_{3/8}$ structures. (b) the band structure of $Hf_2CO_{6/8}S_{2/8}$ structure at mbJ level

Spanish MICIUN/FEDER RTI2018-095460-B-I00 and María de Maeztu MDM-2017-0767 grants. This work was granted access to the HPC resources of TGCC under the allocation 2021-A01008104333 made by GENCI.

Notes and references

1 Naguib, M.; Kurtoglu, M.; Presser, V.; Lu, J.; Niu, J.; Heon, M.; Hultman, L.; Gogotsi, Y.; Barsoum, M. W. Two-Dimensional Nanocrystals Produced by Exfoliation of Ti_3AlC_2. Adv. Mater. **2011**, 23, 4248–4253 https://doi.org/10.1002/adma.201102306

2 Naguib, M.; Mochalin, V.; Barsoum, M. W.; Gogotsi,Y. 25th Anniversary Article: MXenes: A New Family of Two-Dimensional Materials. Adv. Mater. **2014**, 26, 992–1005 https://doi.org/10.1002/adma.201304138

3 Vahid Mohammadi, A. ; Rosen, J.; Gogotsi,Y. The world of two-dimensional carbides and nitrides (MXenes), Science. **2021**, 372, 6547 https://DOI: 10.1126/science.abf1581

4 Anasori,B.; Lukatskaya,M. R.; Gogotsi,Y. 2D Metal Carbides and Nitrides (MXenes) for Energy Storage. Nat. Rev. Mater. **2017**, 2, 16098 https://doi:10.1038/natrevmats.2016.98

5 Morales-García, Á.; Calle-Vallejo, F.; Illas, F. MXenes: New Horizons in Catalysis.ACS Catal **2020**, 10, 22, 13487–13503 doi.org/10.1021/acscatal.0c03106

6 Deeva, E. B.; Kurlov, A.; Abdala, P. M.; Lebedev, D; Kim, S.M.; Gordon, C. P.; Tsoukalou, A.; Fedorov, A.; Mulller, C. R. In Situ XANES/XRD Study of the Structural Stability of Two-Dimensional Molybdenum Carbide Mo_2CT_x: Implications for the Catalytic Activity in the Water-Gas Shift Reaction. Chem. Mater. **2019**, 31, 4505–4513 https://doi:10.1021/acs.chemmater.9b01105

7 Lin, H.; Wang, Y.; Gao, S.; Chen, Y.; Shi, J. Theranostic 2D Tantalum Carbide (MXene). Adv. Mater. **2017**, 30, 992–1005 https://doi:10.1002/adma.201703284

8 Shahzad, F.; Alhabeb, M.; Hatter, C. B.; Anasori, B.; Man Hong, S.; Koo, C. M.; Gogotsi, Y. Electromagnetic Interference Shielding with 2D Transition Metal Carbides (MXenes). Science **2016**, 353, 992-1005 https://doi:10.1126/science.aag2421

9 Sherryna, A.; Tahir, M. Role of Surface Morphology and Terminating Groups in Titanium Carbide MXenes (Ti3C2Tx) Cocatalysts with Engineering Aspects for Modulating Solar Hydrogen Production: A Critical Review Chemical Engineering Journal, **2022**, 433, 134573 doi.org/10.1016/j.cej.2022.134573

10 Naguib, M.; Mashtalir, O.; Carle, J.; Presser, V.; Lu, J.; Hultman, L.; Gogotsi, Y.; Barsoum, M. W.; Two-Dimensional Transition Metal Carbides. ACS NANO **2012**, 6, 1322–1331 https://doi.org/10.1021/nn204153h

11 Radovic, M.; Barsoum, M.W.; MAX phases: Bridgingthe gap between metalsand ceramics. Am Ceram. Soc. Bull. **2013**, 92, 20

12 Caffrey, N. M. Effect of mixed surface terminations on the structural and electrochemical properties of two-dimensional $Ti_3C_2T_2$ and V_2CT_2 MXenes multilayers, Nanoscale. **2018**, 10, 13520-13530 https://doi:10.1039/C8NR03221A

13 Xiong, D.; Li, X.; Bai, Z.; Lu, S. Recent Advances in Layered $Ti_3C_2T_x$ MXene for Electrochemical Energy Storage, Small. **2018**, 14, 1703419 https://doi:10.1002/smll.201703419

14 Liang, X.; Garsuch, A.; Nazar, L.F. Sulfur Cathodes Based on Conductive MXene Nanosheets for High- Performance Lithium–Sulfur Batteries, Angew. Chem. **2015**, 54, 3907-3911 https://doi:10.1002/anie.201410174

15 Liu,X.; Shao, X.; Li, F.; Zhao, M. Anchoring effects of S-

terminated Ti_2C MXene for lithium-sulfur batteries: A First-Principles Study, Applied Surface Science. **2018**, 455, 522-526 https://doi:10.1016/j.apsusc.2018.05.200

16 Suzuki, M.; Suzuki, I.S.; Walter, J. Magnetism and superconductivity in $McTa_2S_2C$ (M = Fe, Co, Ni, and Cu), Phys. Rev. **2005**, 71, 224407 https://doi:10.1103/PhysRevB.71.224407

17 Zha , XH.; Huang, Q.; He, J.; He, H.; Zhai, J. J.S Francisco, S. Du, The thermal and electrical properties of the promising semiconductor MXene Hf_2CO_2, Sci Rep. **2016** , 6, 27971 https://doi.org/10.1038/srep27971

18 Yang, J.; Wang, A.; Zhang, S.; Wu, H.; Chen, L. Stability and electronic properties of sulfur terminated two-dimensional early transition metal carbides and nitrides (MXene), Computational Materials Science. **2018**, 153, 303–308 https://doi.org/10.1016/j.commatsci.2018.07.008

19 Jin, W.; Wu, S.; Wang, Z. Structural, electronic and mechanical properties of two-dimensional janus transition metal carbides and nitrides, Physica E Low Dimens. Syst. Nanostruct. **2018** , 103, 307–313 https://doi.org/10.1016/j.physe.2018.06.024

20 Edirisuriya, M.; Siriwardane, D.; Hu, J. First-Principles Investigation of Ti_2CSO and Ti_2CSSe Janus MXene Structures for Li and Mg Electrodes, J. Phys. Chem. **2021**, 125, 12469–12477 https://doi.org/10.1021/acs.jpcc.1c00082

21 Yang, X.; Qin, X.; Luo, J.; Abbas, N.; Tang, J.; Li, Y.; Gu, K. HfS_2/$MoTe_2$ vdW heterostructure: bandstructure and strain engineering based on first-principles calculation, RSC Adv. **2020**, 10, 2615-2623 (2020). https://doi.org/10.1039/C9RA10087C

22 G.W. King'ori, C.N. M. Ouma, A.K. Mishra, G. O. Amolo , N.W. Makau, Two-dimensional graphene–HfS_2 van der Waals heterostructure as electrode material for alkali-ion batteries, RSC Adv. **10**, 30127–30138 (2020). https://DOI:10.1039/d0ra04725b

23 Singh, D.; Gupta, S. K.; Sonvane, Y.; Kumar, A.; Ahuja, R. 2D-HfS_2 as an efficient photocatalyst for water splitting. *Catal. Sci. Technol.* **2016**, 6, 6605-6614 https://doi.org/10.1039/c6cy01172a

24 Kresse, G.; Joubert, D. From ultrasoft pseudopotentials to the projector augmented-wave method.Phys. Rev. B **1999**, 59, 1758-1775 https://doi.org/10.1103/PhysRevB.59.1758

25 Kresse, G.; Furthmüller, J. Efficiency of ab-initio total energy calculations for metals and semiconductors using a plane-wave basis set. Comput. Mat. Sci. **1996**, 6, 15-50 https://doi.org/10.1016/0927-0256(96)00008-0

26 Kresse, G.; Hafner, J. Ab initio molecular dynamics for liquid metals.Phys. Rev. B **1993**, 47, 558-561, https://doi.org/10.1103/PhysRevB.47.558

27 Perdew, J. P.; Burke, K.; Ernzerhof, M. Generalized gradient approximation made simple. Phys. Rev. Lett. **1996**, 77, 3865-3868 https://doi.org/10.1103/physrevlett.77.3865

28 Morales-García, Á.; Valero, R.; Illas F. An Empirical, yet Practical Way To Predict the Band Gap in Solids by Using Density Functional Band Structure Calculations .Chem. Phys. C **2017**, 121, 34, 18862–18866 https://doi.org/10.1021/acs.jpcc.7b07421

29 Heyd, J.; Scuseria, G. E.; Ernzerhof, M. Hybrid functionals based on a screened Coulomb potential.J.Chem. Phys. **2003**, 118, 8207-8215, https://doi.org/10.1063/1.1564060

30 A. Togo, I. Tanaka, First principles phonon calculations in materials science. *Scr. Mater.* **2015**, 108, 1-5 https://doi.org/10.1016/j.scriptamat.2015.07.021

31 Gonze, X.; Lee, C.; Dynamical matrices, Born effective charges, dielectric permittivity tensors, and interatomic force constants from density-functional perturbation theory. *Phys. Rev. B.* **1997**, 55, 10355 https://doi.org/10.1103/PhysRevB.55.10355

32 Grimme, S.; Antony, J.; Ehrlich, S.; Krieg, H. A consistent and accurate ab initio parametrization of density functional dispersion correction ($DFT-D$) for the 94 elements $H-Pu$.J. Chem. Phys. **2016**, 132, 132-154104 https://doi.org/10.1063/1.3382344

33 Grimme, S.; Ehrlich, S.; Goerigk, v. Effect of the damping function in dispersion corrected density functional theory. *J. Comp. Chem.* **2011**, 32, 1456-1465 https://doi.org/10.1002/jcc.21759

34 Martyna, G. J.; Klein, M. L.; Tuckerman, M. Nose-Hoover chains: The canonical ensemble via continuous dynamics. *J. Chem. Phys.* **1992**, 97, 2635-2643 https://doi.org/10.1063/1.463940

35 Nose, S.; A Molecular Dynamics Method for Simulations in the Canonical, Ensemble. *Mol. Phys.* **1984**, 52, 255–268 https://doi.org/10.1080/00268978400101201

36 Nose, S. A Unified Formulation of the Constant Temperature Molecular Dynamics Methods. *J. Chem. Phys.* **1984**, 81, 511-519 https://doi.org/10.1063/1.447334

37 Jin, W.; Wu, S.; Wang, Z. Structural, electronic and mechanical properties of two-dimensional Janus transition metal carbides and nitrides, Physica E: Low-dimensional Systems and Nanostructures. **2018**, 18, 30440-5 https://DOI:10.1016/j.physe.2018.06.024

38 Wang, Y.; Ma, S.; Wang, L.; Jiao, Z. A novel highly selective and sensitive NH_3 gas sensor based on monolayer Hf_2CO_2, Appl. Surf. Sci. **2019**, 492, 116-124 https://doi:10.1016/j.apsusc.2019.06.212

39 Gandi, A.N. ; Alshareef, H.N.; Schwingenschlögl, Udo Thermoelectric Performance of the MXenes M_2CO_2 (M = Ti, Zr, or Hf), Chem. Mater. **2016**, 28, 1647-1652 https://doi.org/10.1021/acs.chemmater.5b04257

40 Hartmut , Z.; Mechanical properties of graphene and boronitrene, J. Phys.: Condens. Matter, **1999**, 11, 9303-9346 https://doi:10.1103/physrevb.85.125428

41 Peng, Q.; De, S. Outstanding mechanical properties of monolayer MoS_2 and its application in elastic energy storage, Phys. Chem. Chem. Phys. **2013** , 15, 19427-19437 https://doi.org/10.1039/C3CP52879K

42 Peelaers, H.; Van de Walle, C. G. Elastic Constants and Pressure-Induced Effects in MoS_2, J. Phys. Chem. C **2014**, 118 , 12073–12076 https://ddoi.org/10.1021/jp503683h

43 Guo, Z.; Zhou, J0.; Zhu, L.; Sun, Z. MXene: A promising

photocatalyst for water splitting, J. Mater. Chem. A, **2016** , 4 ,511-519 https://doi.org/10.1039/C6TA04414J

44 Zha, X. H.; Huang, Q.; He, J.; He, H.; Zhai, J.; Wu, Y.; Francisco, J.S.; Du, S. The thermal and electrical properties of the promising semiconductor MXene Hf_2CO_2, Scientific Reports. **2016**, 6 , 27971 https://doi:10.1038/srep27971 J

45 Zhang, Y.; Xia, W.; WU, Y. ; Zhang, P. Prediction of MXene based tunable band gap 2D semiconductors: GW quasiparticle calculations Nanoscale. **2019**, 11 , 3993-4000 https://DOI https://doi.org/10.1039/C9NR01160AJ

46 Sun, X.; Mi, Y.; Jiao, F.; Xu, X. Activating Layered Perovskite Compound Sr_2TiO_4 via La/N Codoping for Visible Light Photocatalytic Water Splitting, ACS Catal. **2018**, 8, 3209-3221 https://doi.org/10.1021/acscatal.8b00369J

47 Bader, R. F. W. Atoms in molecules: A quantum theory, ed. Clarendon Press: Oxford, U. K., **1990**, 438.

48 Ouahrani, T.; Merad-Boudia, I.; Baltache, H.; Khenata, R.; Bentalha, Z. Effect of pressure on the global and local properties of cubic perovskite, crystals Phys. Scr. **2011**, 84 ,025704 https://doi.org/10.1088/0031-8949/84/02/025704

49 Johnson, E. R.; Keinan, S.; Mori-Sanchez, P.; Contreras-Garcia, J.; Cohen, A.J.; Yang, W.; Revealing noncovalent interactions, J. Am. Chem. Soc. **2010**, 132 , 6498-6506 https://doi.org/10.1021/ja100936w

50 Guedda, H. Z.; Ouahrani, T.; Morales-García, A.; Franco, R.; Salvadó,M. A.; Pertierra, P.; Recio, J. M. Computer simulations of 3C-SiC under hydrostatic and non-hydrostatic stresses, Phys. Chem. Chem. Phys. **20016**, 18, 8132-8139 https://doi.org/10.1039/C6CP00081A

51 Mori-Sanchez, P.; Pendas, A. M.; Luana, V.; A classification of covalent, ionic, and metallic solids based on the electron density, J. Am. Chem. Soc. **2002**, 124, 14721 https://doi.org/10.1021/ja027708t

52 Bouheddadj, A.; Ouahrani, T.; Kannounou, G. W.; Reda, B.; Bedrane, S.; Badawi, M. A. Morales-Garcia, Low-dimensional HfS_2 as SO_2 adsorbent and gas sensor: Effect of water and sulfur vacancies, Phys. Chem. Chem. Phys. **2021**, 23, 23655-23666 https://DOI: 10.1039/D1CP04069C

53 Karlsson, L.H.; Birch, J.; Halim, J.; Barsoum, M.W.; Persson, P.O. Atomically resolved structural and chemical investigation of single MXene sheets, Nano Letters 15 **2015**, 15, 4955–4960 https://doi.org/10.1021/acs.nanolett.5b00737

54 Hu, T.; Wang, J.; Zhang, H.; Li, Z.; Hu, M.; Wang, X. Vibrational properties of Ti_3C_2 and $Ti_3C_2T_2$ (T = O, F, OH) monosheets by first-principles calculations: a comparative study, Physical Chemistry Chemical Physics. **2015**, 17, 9997-10003 https://doi.org/10.1039/c4cp05666c

55 Yu,X.; Yohan, D.A.; Michael, N.; Yury, G.; Barsoum, M.W.; Zhuang, H.L.; Kent, P.R.C. Prediction and characterization of MXene nanosheet anodes for non-lithium-ion batteries, ACS Nano. **2004** , 8, 9606-9615 https://doi.org/10.1021/nn503921j

56 Wang, X.; Shen, X.; Gao, Y.; Wang, Z.; Yu, R.; Chen, L. Atomic-scale recognition of surface structure and intercalation mechanism of Ti_3C_2X, Journal of the American, Chemical Society. **20015**, 137, 2715-2721 https://doi.org/10.1021/ja512820k

57 Maria, L.R.; Olha, M.; Chang, R.E.; Yohan, D.A.; Patrick, R.; Pierre Louis, T.; Michael, N.; Patrice, S.; Michel, B.W.; Yury, G. Cation intercalation and high volumetric capacitance of two-dimensional titanium carbide, Science. **2013**, 341, 1502-1505 https://doi.org/10.1126/science.1241488

58 Berbel, M. L.; Morales-Garcia, A.l; Viñes, F.; Illas, F. Thermodynamics and Kinetics of Molecular Hydrogen Adsorption and Dissociation on MXenes: Relevance to Heterogeneously Catalyzed Hydrogenation Reactions, ACS Catalysis. **2021**, 21 , 112850–1285 DOI: 10.1021/acscatal.1c03150

59 Tang, Q.; Zhou, Z.; Shen, P. Are MXenes promising anode materials for Li ion batteries computational studies on electronic properties and Li storage capability of Ti_3C_2 and $Ti_3C_2X_2$ (X = F, OH) monolayer, Journal of the American Chemical Society. **2012**, 134, 16909-16916 https://doi.org/10.1021/ja308463r